

Pressure-induced amorphization, crystal-crystal transformations and the memory glass effect in interacting particles in two dimensions

S. Bustingorry¹ and E. A. Jagla²

¹*Centro Atómico Bariloche and Instituto Balseiro,
Comisión Nacional de Energía Atómica, (8400) Bariloche, Argentina*
²*The Abdus Salam ICTP, Strada Costiera 11, (34014) Trieste, Italy*

(Dated: November 13, 2018)

We study a model of interacting particles in two dimensions to address the relation between crystal-crystal transformations and pressure-induced amorphization. On increasing pressure at very low temperature, our model undergoes a martensitic crystal-crystal transformation. The characteristics of the resulting polycrystalline structure depend on defect density, compression rate, and nucleation and growth barriers. We find two different limiting cases. In one of them the martensite crystals, once nucleated, grow easily perpendicularly to the invariant interface, and the final structure contains large crystals of the different martensite variants. Upon decompression almost every atom returns to its original position, and the original crystal is fully recovered. In the second limiting case, after nucleation the growth of martensite crystals is inhibited by energetic barriers. The final morphology in this case is that of a polycrystal with a very small crystal size. This may be taken to be amorphous if we have only access (as experimentally may be the case) to the angularly averaged structure factor. However, this ‘X-ray amorphous’ material is anisotropic, and this shows up upon decompression, when it recovers the original crystalline structure with an orientation correlated with the one it had prior to compression. The memory effect of this X-ray amorphous material is a natural consequence of the memory effect associated to the underlying martensitic transformation. We suggest that this kind of mechanism is present in many of the experimental observations of the memory glass effect, in which a crystal with the original orientation is recovered from an apparently amorphous sample when pressure is released.

PACS numbers: 64.70.Kb, 61.50.Ks, 61.43.-j

I. INTRODUCTION

Several crystalline materials are known to become amorphous under changes of the ambient pressure,^{1,2,3} and this may occur under compression or decompression. Among the most thoroughly studied cases, due to its technological or geophysical importance, we find H₂O, SiO₂, GeO₂, AlPO₄ and other isostructural compounds. The occurrence of pressure induced amorphization (PIA) is characteristic of (although not limited to) tetrahedrally coordinated materials.

The simple statement that a material becomes amorphous under pressure covers a broad range of different experimental situations and possible theoretical interpretations. The simplest possibility is a crystalline material that transforms (upon change of the external pressure) to a completely amorphous structure when a well defined transition pressure is reached. We will call this possibility true PIA (TPIA). This strict case of PIA is by no means the only possible one. A reason for this is that typically PIA is claimed to occur (on an experimental basis) when the obtained sample does not display sharp X-ray diffraction peaks. We will refer to these samples as ‘X-ray amorphous’ material. A relatively large amount of local order can still be present in an X-ray amorphous. For instance, a polycrystal with a sufficiently small crystal size is an X-ray amorphous material. An eventual transition from a single-crystal sample to this kind of polycrystal should be considered, on an experimental basis, to be a

PIA transition. This is a second case of PIA that we will call ‘weak’ (WPIA).

Experimentally, WPIA or some variants of it may be the rule more than the exception. It is seen in many cases that amorphization occurs through a sequence of transformations in which one or more intermediate crystalline phases can be identified. For instance, a crystal-crystal pressure induced transformation was shown to occur in α -quartz between 21 and 30 Gpa^{4,5,6}. The new crystalline phases, quartz II and a $P2_1/c$ phase, may be intermediate states in the path toward complete amorphization, occurring at higher pressures. Yet, the final amorphous material may well be only an X-ray amorphous material.

A common characteristic of both WPIA and TPIA is that the starting crystalline sample becomes unstable upon pressure. This instability does not typically disappear if temperature is reduced. This is an indication that in most, if not all cases, the mechanisms of PIA can be discussed in the limit of $T = 0$. In this limit, all structural transformations that may eventually occur are of a mechanical nature, i.e., the displacement of the particles during the transformation is strictly guided by the tendency of the system to minimize its mechanical energy. In addition to being a simplifying assumption, the consideration of vanishingly small temperature is conceptually important, as in this case structural transformations are necessarily related to mechanical instabilities in the system. We notice that although we will present all our

analysis at $T \sim 0$, this is in principle applicable also to any temperature below the glass transition temperature T_g of the fluid phase, where diffusion effects are negligible. We only need to consider in this case that the parameters of the model may depend on temperature. Since at $T < T_g$ diffusive processes are almost totally inhibited, any structural transition (in particular, PIA) occurring in this temperature range is of a displacive nature. This raises the question of the relation between PIA and martensitic transformations.⁷ In fact, the discussion of the similarities between PIA and martensitic transformations is one of the main aims of the present paper.

There is also a long standing controversy about whether PIA is of a mechanical or thermodynamical nature,^{2,8,9,10,11,12} and this in turn is related to the two possible mechanisms of melting at higher temperatures: mechanical or thermodynamical.¹³ Thermodynamical melting implies the growth of the fluid phase when it starts to be more stable than the solid phase. This growth is heterogeneous and occurs in the presence of extended nucleation centers, such as grain boundaries or even the surface of the sample. If these defects do not exist (something that can be achieved in numerical simulations by the use of single-crystalline samples with periodic boundary conditions), then the fluid phase is not able to nucleate until the ultimate mechanical equilibrium conditions are violated. This is known as Born's mechanical stability criteria, and the melting mechanism in this limit is called mechanical melting. Mechanical melting is homogeneous, as it affects the whole sample at the same time, and occurs very rapidly once the stability limit is reached. It has been suggested that these two melting mechanisms can be extended to describe two different amorphization mechanisms.¹³

There are quite a few numerical models devised to study PIA in different materials. In some cases, a thorough description of a particular material is pursued. In this case, the models range from first principle density functional calculations^{14,15} to molecular dynamics simulations with different pair-potential interactions.^{16,17,18} Within these models, PIA can be directly studied in concrete systems such as H_2O or SiO_2 . A more qualitative approach is obtained by using core-softened potentials,^{19,20} which proved to be very useful for the study of water-like anomalies and polyamorphism in tetrahedrally coordinated materials.^{21,22,23,24,25} The aim of this approach is not to carry out an analysis of the properties of a specific material, but to find out general trends and qualitative behaviors that shed light on the properties of a large family of materials. This is the approach that we will follow here.

We study here a two-dimensional model of identical particles interacting through a spherically symmetric two body potential. We have recently shown that choosing appropriately the interaction potential, the model presents TPIA upon pressure release if we start from the stable high pressure phase.²⁶ Here we analyze in detail

the WPIA that occurs when we increase pressure starting from the stable low pressure phase. We show that this transformation is of a martensitic nature, and analyze the nucleation and growth of the crystallites of the new phase. Depending on details of the potential, two different extreme possibilities occur. In one of them, the new phase grows in large crystallites of the (three) different martensitic variants, and crystallites grow perpendicularly to the habit line of the martensitic transformation. This is a case of ideal martensitic transformation. In the other limiting case, the new crystallites nucleate but can hardly grow. In this case, a WPIA scenario is realized. The final sample is X-ray amorphous, but it conserves a memory of its original starting configuration. This memory manifests upon pressure release: the sample recovers (partially) the orientation it had prior to compression. We discuss the characteristics of the interaction potential that are responsible for the different behavior.

The paper is organized as follows. In Sec. II, we present the model and details of the performed numerical simulations. The ideal martensitic transformation is introduced in Sec. III. In Sec. IV, we describe the martensitic transformation for the case when low energy barriers are involved in the growth process. The case were this energy barriers are higher, which leads to a WPIA, is discussed in Sec. V. Finally, Sec. VI contains some discussion and conclusions.

II. THE MODEL, NUMERICAL DETAILS AND EQUILIBRIUM PROPERTIES

We consider a two-dimensional system of particles, interacting through a specially devised isotropic, purely repulsive pairwise potential. Its main characteristic is the existence of two competing distances r_0 and $r_1 > r_0$ at which neighbor particles prefer to be located, depending on the applied pressure. This kind of core-softened potential has been previously used to study anomalous properties of tetrahedrally coordinated materials,^{21,22,24,25} and it was recently used to study the TPIA case also.²⁶ The interaction potential $V(r)$ between two particles separated a distance r is explicitly given by^{24,26}

$$\begin{aligned} V(r) &= \frac{\varepsilon}{0.81} [8(r/a - 1.55)^2 + 16(r/a - 1.55)^4 + \\ &\quad w(r/a - 2)^2 + 0.81] \text{ for } r < 2a \\ &= 0 \text{ for } r > 2a \end{aligned} \quad (1)$$

Here, ε and a fix the energy and length scales, and w is a control parameter that allows us to change the height of the shoulder of the interparticle potential (see Fig. 1). Neighbor particles prefer to be located on both sides of the shoulder, in the positions qualitatively indicated in Fig. 1 as r_0 and r_1 . Simulation results will be presented mainly for $w = 6$ and $w = 10$ to assess the effect of the barrier height on the morphology of the microstructure

obtained. Note that, although for $w = 10$ the curvature of the interparticle potential does not change sign, the potential gives rise to two preferred distances when analyzing two- or three-dimensional configurations.

The system is simulated by standard molecular dynamics in the NVT ensemble.^{27,28} This choice allows us to survey all regions of the volume-pressure curve, including those that would be unstable in constant pressure simulations. We perform simulations with 9540 particles, with a time step of $\delta t = 0.01t_0$ (where $t_0 = a\sqrt{m/\varepsilon}$ is the time unit, m being the mass of each particle). Pressure and elastic constant are calculated along the simulations using standard formulas (see the Appendix for details). We always use periodic boundary conditions (PBC). This is a particularly convenient choice when we want to avoid the heterogeneous nucleation of the new phase. On the contrary, in the case in which we study the heterogeneous nucleation, we introduce the nucleation centers by hand in the crystalline structure. The use of PBC in this case does not impose any strong additional restriction in the possible transformations to be observed, as our systems contain enough atoms to accommodate essentially any possible new phase, even using PBC.

The volume of the system is changed at a fixed rate during the simulation. This change is done by rescaling all coordinates of the particles and size of the simulation box. The volume change rate is taken to be as low as possible (within reasonable computational time) to simulate a quasistatic process. However, it is of course a very large rate in physical units. For instance, a typical volume change rate we use is $10^{-4}t_0^{-1}$, and for an atomic particle ($t_0 \sim 10^{-15}s$) this implies a rate of the order of 10^{-2} per femtosecond.

By rescaling down the velocities of the particles during the simulation, temperature is kept constant at a very small value of the order of $10^{-5}\varepsilon$ (we take the Boltzmann constant to be unity). As the transformation process implies local mechanical instabilities, there is a systematic transformation of potential energy into kinetic energy. In experiments, this reflects an increase of the temperature of the system. Here the kinetic energy excess is taken away through the mentioned velocity rescaling procedure.

We emphasize that the use of a two-dimensional system is dictated by the simplicity of the simulation and also of the interpretation of the results. While we expect the same qualitative kind of results to reappear in full three dimensional systems, the computational time increases noticeably, and the adequate identification of the phases becomes much more involved. Note that in a previous work it has been shown that the number of equilibrium solid phases noticeably increases when passing from two to three dimensions,²⁹ then adding to the complexity of the three-dimensional case.

One of the most striking properties of particles interacting through the potential described in the previous section is that the stable crystalline ground state is not necessarily the triangular lattice. In fact, although at low

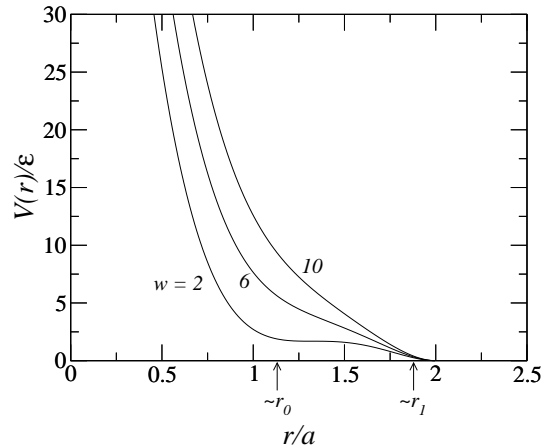


FIG. 1: Pairwise core-softened interparticle potential used in the present work [from Eq. (1)]. The distances r_0 and r_1 are schematically shown.

(high) pressures the ground state of the system is a triangular structure with a lattice parameter around r_1 (r_0), at intermediate pressures lower energy configurations can be obtained that have some of its first neighbors at distances $\sim r_0$, and some others at $\sim r_1$. By increasing the pressure, the configuration to which the low density triangular (LDT) structure is expected to transform is the chainlike (CH) structure.²¹ This is the transition that we will be mostly interested in, and we will analyze it for two different values of w , namely $w = 10$ and $w = 6$. We will see that there are noticeable differences between the two cases.

III. THE IDEAL MARTENSITIC TRANSFORMATION

We will study the behavior of the LDT phase upon volume reduction. The LDT-CH transformation admits a natural description as a martensitic transformation as depicted in Fig. 2. In this description, the LDT corresponds to the austenite phase, and the CH to the martensite phase. Upon volume reduction, the martensite phase becomes stable above the equilibrium transition pressure P^e . Two structures can coexist at this pressure, namely a LDT structure with lattice parameter r^e [Fig. 2(a)], and a CH structure (corresponding to an oblique two-dimensional Bravais lattice) with parameters r_0^e , r_1^e , and β^e [Fig. 2(b)]. To minimize the interface energy at the equilibrium pressure, the two structures have to match along a particular line, called the invariant line or habit line (habit plane in three dimensions, line AB in Fig. 2). This line is determined from the condition that both phases are unstrained away from it.⁷ A relative rotation of the two phases is necessary in order to define the invariant line. The orientation of the invariant line can be easily evaluated given the parameters of the martensite

TABLE I: Structural parameters at the LDT-CH equilibrium point (see Fig. 2 for definitions of the crystallographic parameters), along with the pressure and volume values at the mechanical instability. The angles θ^e and ϕ^e correspond to a relative rotation of the two phases and a reference angle between the invariant line and the LDT structure, respectively (see Fig. 2).

Parameter	$w = 6$	$w = 10$
$P^e a^2 / \varepsilon$	4.83	8.55
v^e / a^2 (LDT)	3.01	2.74
r^e / a (LDT)	1.86	1.78
v^e / a^2 (CH)	2.29	2.38
r_0^e / a (CH)	1.25	1.37
r_1^e / a (CH)	1.93	1.87
β^e (CH)	71.07	68.56
θ^e (CH)	1.46	1.65
ϕ^e (CH)	5.47	9.43
$P^c a^2 / \varepsilon$	6.38	9.34
v^c / a^2	2.76	2.64

and the austenite phase. The structural parameters of the austenite (LDT) and martensite (CH) phases at the equilibrium pressure are given in Table I.

The ideal transformation between the LDT and CH structures does not imply bond breaking, which means that each particle conserves the same first neighbors in the two phases. This implies microscopic memory in the sense that each local neighborhood transforms back to exactly the original configuration upon decompression. Furthermore, this implies that after a cyclic LDT-CH-LDT transformation, the original structure is recovered with the same initial orientation. This property is directly related to the shape memory effect of martensites.

If an invariant line separating the two coexisting phases has formed at the transformation pressure, the transformation can proceed as volume is reduced by reaccommodating particles of the austenite close to the interface to fit into the sites of the martensite.³⁰ The advance of the interface occurs through the lateral movement of the steps that form the interface, and at the equilibrium pressure it implies the surmounting of an energy barrier. Then, at $T = 0$ a small overpressure is necessary to climb this energy barrier. As we will see, this ideal growth mechanism in the direction perpendicular to the invariant line becomes more complicated when strains are involved, and depends strongly on the height of the barrier for the transformation between the austenite and martensite phases.

IV. NUCLEATION AND GROWTH IN THE CASE OF A LOW-ENERGY BARRIER

The previous ideal description of the martensitic transformation can differ from the actual way in which the martensite nucleates and grows from the pure austenite phase in a real situation. In this section, we study this

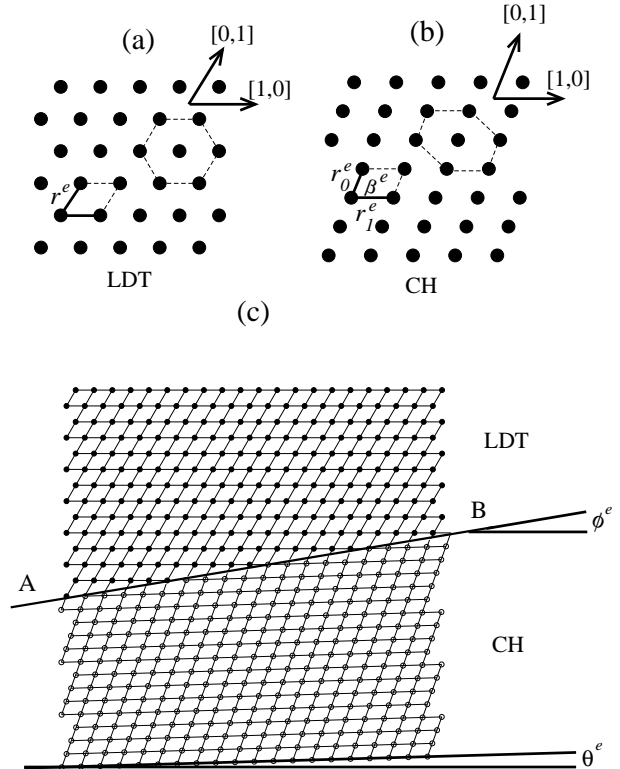


FIG. 2: Ideal (a) LDT and (b) CH structures. The lattice parameter and the crystallographic directions are shown, together with the perfect and distorted hexagonal unit. (c) Interphase between the LDT and CH structures at equilibrium. The invariant line AB is rotated ϕ^e with respect to the LDT structure. The $[1, 0]$ direction of the CH structure is rotated θ^e with respect to the $[1, 0]$ direction of the LDT structure.

process using the potential in Fig. 1 with $w = 10$. On increasing pressure, the low density triangular structure becomes thermodynamically unstable against the chain-like structure beyond P^e . However, as this transformation is first order, at $T = 0$ the perfect LDT structure survives in a metastable state at higher pressures until it finally becomes mechanically unstable. For the case of a perfect (without defects) starting sample, we call the instability pressure P^c (and the corresponding specific volume v^c). The mechanical stability limit corresponds to the value of pressure at which one of the normal modes (phonons) of the original structure first destabilizes. The calculation of the phonon structure of the triangular lattice is straightforward. For our model potential Eq. (1) interactions with second and further neighbors are identically zero, and the stability condition can be written

as

$$\frac{\partial^2 V}{\partial r^2} + \frac{3}{r} \frac{\partial V}{\partial r} > 0, \quad (2)$$

where r is the nearest neighbor distance of the triangular lattice. At the instability pressure P^c , three equivalent shear phonon branches become zero energy. They correspond to shear phonons in the three equivalent directions $[0, 1]$, $[1, 0]$, and $[-1, 1]$ (Fig. 2). Note that, due to the lack of next nearest neighbors interactions, the phonon branch along these directions is of the type $\sim \sin(k)$, and at P^c the whole phonon branch becomes dispersionless.

The fact that the destabilization is initiated by a shear phonon is consistent with an analysis in terms of Born inequalities³¹. In fact, condition (2) is equivalent to the generalization of Born stability criteria to stress dependent conditions^{32,33} in the static (zero temperature) limit. In two dimensions, the Born stability criteria establish that a system is stable if the stress dependent shear modulus $G' = (C_{11} - C_{12})/2 - P$ is positive³³. For the zero temperature case $G' = \sqrt{3}/4[V''(r) + 3V'(r)/r]$ (see Appendix), and then the Born stability criteria reduce to condition (2).

The results of numerical simulation [Fig. 3(a)] confirm the previous analysis. Starting from a perfect triangular structure at zero temperature, once the system reaches the instability volume v^c , the triangular configuration destabilizes and a new stable configuration should emerge. The evolution of the stress dependent shear modulus upon volume decrease is shown in Fig. 3(b), where it is clear that it vanishes at the mechanical instability point.

The consideration of a perfect sample without defects is important in order to realize the equivalence of the mechanical instability limit with the vanishing of the energy of a phonon mode. Moreover, in the present case it also coincides with the vanishing of an elastic constant (a long wave length elastic constant), because of the lack of interactions to next nearest neighbors.³⁴ But certainly, a defect free sample is not typically encountered in experiments. It is important to realize that even tiny amounts of defects can produce important changes in the triggering of the transformation. For instance, a single vacancy can destabilize the lattice at pressures much lower than P^c . This was shown already in the case of TPIA,²⁶ and it is also true here. The evolution of pressure upon volume decrease for a lattice with a single vacancy is also shown in Fig. 3(a). We see that a single vacancy is able to destabilize the original triangular lattice without essentially any pressure overshooting. Note, however, that the inclusion of a single vacancy has no appreciable effect on the values of the shear modulus prior to the transition [Fig. 3(b)]. This means that even in the presence of tiny amounts of disorder, the examination of the elastic constants (or even of the whole phonon spectrum) will not indicate the approach to the instability point. In fact, the instability occurs because of the destabilization of localized modes close to the defect, which have no effect

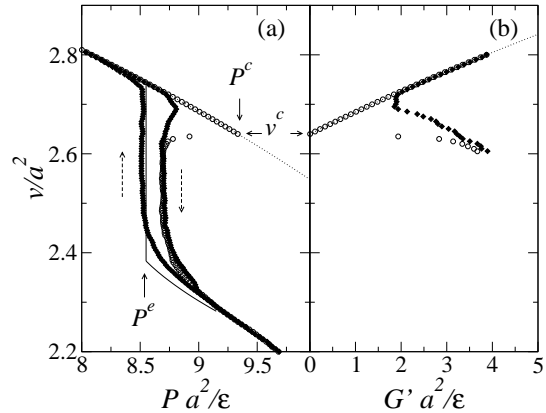


FIG. 3: (a) Volume-pressure curves for $w = 10$. The dotted line is the analytic expression for the evolution of the LDT structure if this remains stable, and the thin continuous line marks the equilibrium transition to the CH structure and the subsequent evolution of this structure. The full and open symbols correspond to simulations with and without a vacancy in the original sample. Vertical dashed arrows indicate the compression-decompression paths. (b) Evolution of the stress dependent shear modulus $G' = (C_{11} - C_{12})/2 - P$ upon decompression for $w = 10$. The dotted line is the analytical result for G' evaluated for the perfect triangular lattice (see the Appendix). Note how in the defect free case, the approach to the transition point ($v \rightarrow v^c$) is signaled by the vanishing of the stress dependent shear modulus.

on the spectrum of the (extended) phonons. The absence of macroscopic effects signaling the approach to the instability is usually associated to thermally activated first order transitions. We see that a similar phenomenology occurs here in the absence of thermal fluctuations, and within a scenario of a transition driven only by mechanical instabilities.

In Fig. 4, a sequence of snapshots is shown to follow the morphology of the transformed regions in the case in which a single vacancy is present in a monocrystalline sample. We can see that the first instability produces the collapse of adjacent rows of particles, around the defect. These collapses generate three platelets that propagate out of the vacancy [Fig. 4(a)]. The collapse directions in the three platelets are different, and are related to the three different variants of the martensitic transformation. In this stage, the martensite crystallites are compressed in the longitudinal direction, in order to match the lattice parameter of the original triangular structure.³⁰ In a subsequent stage [Fig. 4(b),(c)], the new crystallites reaccommodate to take the form of wedge shaped crystallites, with the interface between the martensite and austenite phase being very close to the ideal habit line of the transformation. Then upon further compression [Fig. 4(c-e)] the crystallites grow perpendicularly to the habit line, very much as described for the ideal case in the pre-

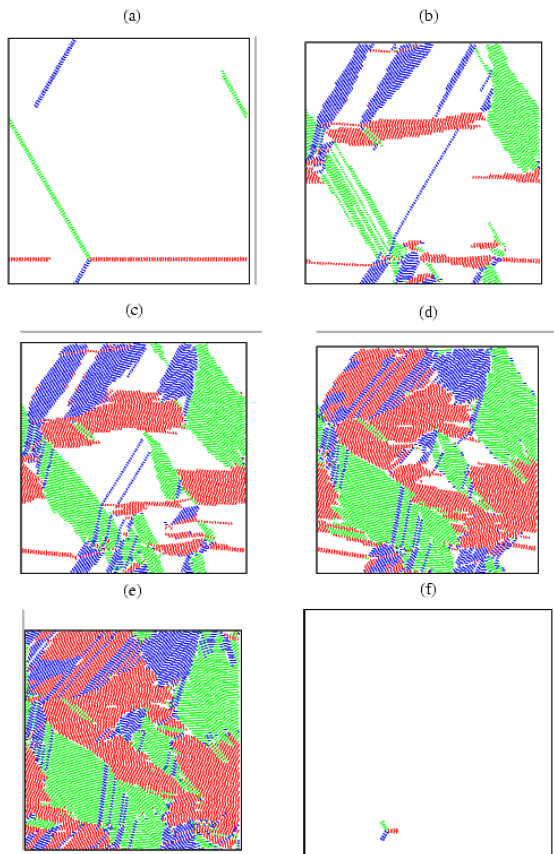


FIG. 4: (Color online) Snapshots of the system with $w = 10$ corresponding to: (a) $v/a^2 = 2.7$, (b) $v/a^2 = 2.6$, (c) $v/a^2 = 2.5$, (d) $v/a^2 = 2.4$, (e) $v/a^2 = 2.3$, on compression, and (f) $v/a^2 = 2.8$ after decompression from the configuration in (e). Only collapsed particles are shown joined by segments, with three different colors to identify the three different variants of the martensite (intact austenite is not plotted for clarity). The starting system contains a single vacancy at the position where the three different variants start nucleating in (a). Note that periodic boundary conditions are used.

vious Section. The final state of the system (when the whole sample has transformed to the martensitic phase) consists of a polycrystalline sample with the three different orientation of the possible variants [Fig. 4(e)]. Note from Fig. 3(a), that after nucleation, pressure has remained essentially constant during the whole transformation from the LDT to the CH structure, at a value slightly larger than the equilibrium value. This value reflects the overpressure needed to keep the transformation proceeding.

If the volume of the system is increased back starting from the sample completely in the martensitic phase, upon complete pressure release essentially any particle in the system returns to its original position, in which it has exactly the same neighbors as before compression. In particular, this implies that the original monocrystalline

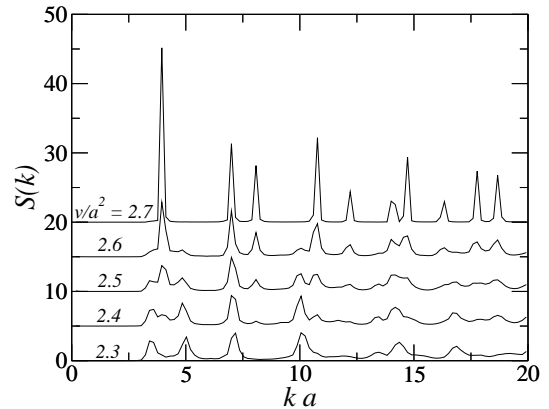


FIG. 5: Evolution of the averaged structure factor $S(k)$ with decreasing volume for the LDT-CH transformation with $w = 10$ (the curves are vertically displaced, for clarity). Different curves correspond to the configurations in Fig. 4 (a)-(e).

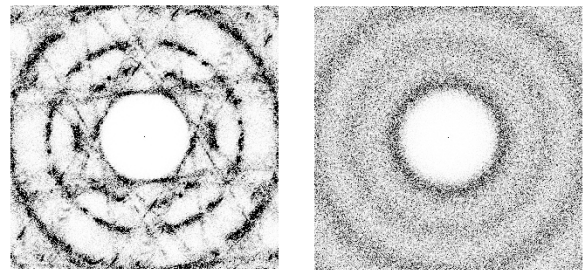


FIG. 6: Two-dimensional (upper) and angularly averaged (lower) structure factors of the configuration in Fig. 4(e), and of the configuration obtained by quenching from the melt at the same density. In the top, the two-dimensional structure factors of the polycrystalline CH structure (left) and quenched amorphous structure (right) are shown. In the lower figure, bold and thin lines correspond to the averaged $S(k)$ for the polycrystalline CH and quenched amorphous structures, respectively. There is a clear crystallinity observable in the first case, even if we look only at the radial structure function. This sample should be characterized as polycrystalline.

austenite sample is reobtained, with the same orientation as in the starting configuration.³⁵ This is not a surprise, since it is in the essence of the shape memory effect of martensites. It can be seen in Fig. 3(a) that the return occurs with a noticeable hysteresis with respect to compression. This hysteresis is a consequence of the individual hysteresis of pairs of neighbor particles on passing between the two equilibrium distances, and can be used to quantify the energy dissipated during a compression-decompression cycle.

Now we want to discuss how the transformation manifests when we observe the diffraction patterns of the structures. In Fig. 5 we show the angularly averaged structure factor $S(k)$ corresponding to the configurations in Fig. 4(a)-(e). It is possible to see how some characteristic peaks of the LDT structure progressively disappear while new peaks appear that correspond to the CH structure. A broadening of the peaks is also apparent, due to the finite size of the crystallites in the new configuration. This broadening however is not large enough to consider the sample as X-ray amorphous. By comparing the structure factor of this structure with that of a sample obtained by quenching from the melt at the same density (Fig. 6), we first observe that the two-dimensional structure factor displays clear evidence of the polycrystalline character of the sample. But even if we look only at the radial structure factor, there are much sharper peaks for our sample compared to the quenched liquid. Then the configuration in Fig. 4(e) can be correctly identified from its structure factor as a polycrystalline sample.

V. BLOCKED GROWTH FOR LARGE ENERGY BARRIER

In the present section, we will study the modification brought upon by a change of the parameter w of the potential. The value used here is $w = 6$. In principle, the same description of the ideal martensitic transformation is valid also in this case. The value of the crystallographic parameters are given in Table I. In Fig. 7(a), we show the volume-pressure evolution of the volume controlled compression for $w = 6$. Open symbols correspond to the starting sample without defects. The simulation shows that the system remains in the triangular structure until the mechanical stability limit (P^c, v^c) is reached. On the contrary, the sample with a single vacancy begins to transform when local mechanical instabilities occur, before reaching the mechanical stability limit. The behavior of the stress dependent shear modulus for the present case, with and without the vacancy, is shown in Fig. 7(b). The phenomenology up to here is very similar to the case of the previous section. However, important differences appear when we look at the morphology of the samples and the structure factors. We again focus on the case of a system with a single vacancy. In Fig. 8, snapshots of the system as volume is decreased are shown. As in the previous case, the first elements of the new phase to

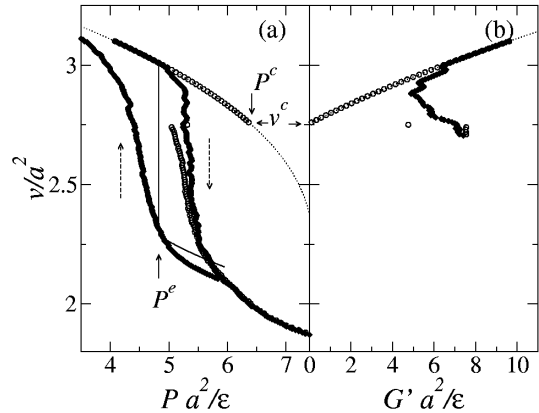


FIG. 7: (a) Volume-pressure curves for $w = 6$. The dotted line is the expected evolution of the LDT structure, and the thin continuous line marks the equilibrium transformation to the CH structure and the subsequent evolution of the new structure. The full and open symbols correspond to simulations with and without a vacancy in the original sample. Vertical dashed arrows indicate the compression-decompression paths. (b) Evolution of the stress dependent shear modulus $G' = (C_{11} - C_{12})/2 - P$ upon decompression for $w = 6$. The dotted line corresponds to G' evaluated from the interatomic potential (see the Appendix). P^c and v^c are given by the vanishing of the stress dependent shear modulus in (b) (see Table I).

be nucleated are the platelets starting at the position of the vacancy. But contrary to the previous case, they do not rearrange to generate an interface along a habit line. As the growth process in these conditions implies much higher overpressure, the growth remains mostly blocked, and upon further compression nucleation of new platelets throughout the sample occurs. New and old platelets interact elastically, and deform each other, generating at the end a structure that in spite of being martensitically related to the original one, contains crystallites that are extremely small.

On very general grounds, since our polycrystalline structure has very small crystallites, a broadening of the characteristic peaks of the azimuthally averaged X-ray pattern is expected.³⁶ There is a continuous crossover however from this ‘broadened peaks’ scenario, to one in which no sharp peaks are observed. In the last case the sample should be characterized as X-ray amorphous. But even in this case it can possess specific crystal characteristics, and in particular it may conserve a structural relation with the parent structure that will manifest upon decompression.

In Fig. 9, we show angularly averaged structure factors corresponding to the configurations shown in Fig. 8 (a)-(e). Again, the peaks of the LDT structure disappear while reducing the volume, but the intensity of the peaks corresponding to the CH structure is much weaker than

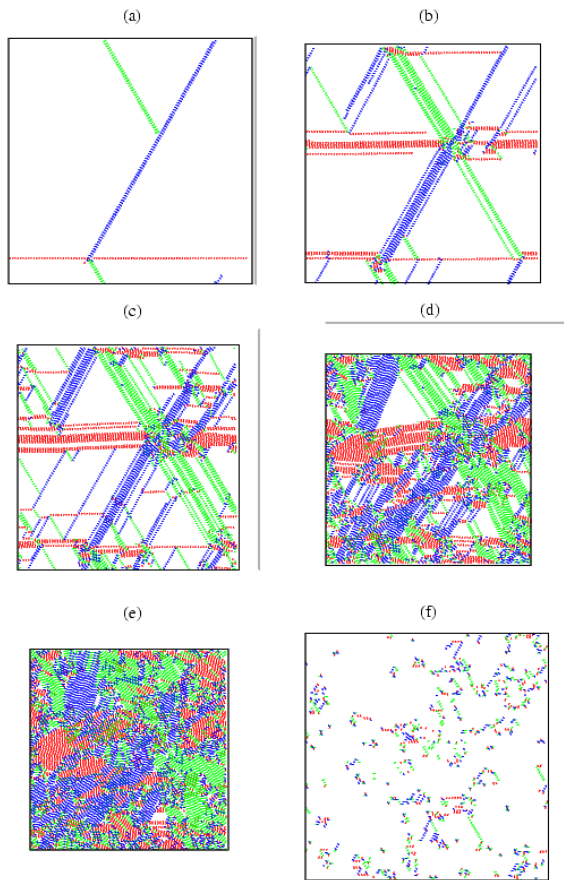


FIG. 8: (Color online) Snapshots of the volume controlled simulation of the system with $w = 6$ corresponding to: (a) $v/a^2 = 2.95$, (b) $v/a^2 = 2.8$, (c) $v/a^2 = 2.6$, (d) $v/a^2 = 2.3$, (e) $v/a^2 = 2.1$, on compression, and (f) $v/a^2 = 3.05$ on decompression from $v/a^2 = 2.1$. Only collapsed particles are shown joined by segments, with three different colors to identify the three different variants of the martensite (intact austenite is not plotted for clarity). The starting system contains a single vacancy at the position where the three different variants start nucleating in (a). Note that periodic boundary conditions are used.

in the $w = 10$ case. In Fig. 10 the two-dimensional X-ray diffraction patterns of the structure obtained from a single crystal LDT sample, and an amorphous structure obtained by quenching from the melt (with the same density), are shown. We see that the two-dimensional pattern of the sample obtained by compression possesses an angular structure reminiscent of the original crystal orientation (in fact, this structure will be responsible for a ‘memory effect’ when the sample is decompressed, see below). However, if our starting sample is already polycrystalline, as is usually the case experimentally, the X-ray pattern is by definition isotropic. In that case all the information available is the radial X-ray pattern. The angularly averaged $S(k)$ are shown at the bottom of Fig. 10. On the basis of the $S(k)$ function, the compressed sample cannot be clearly distinguished from that obtained

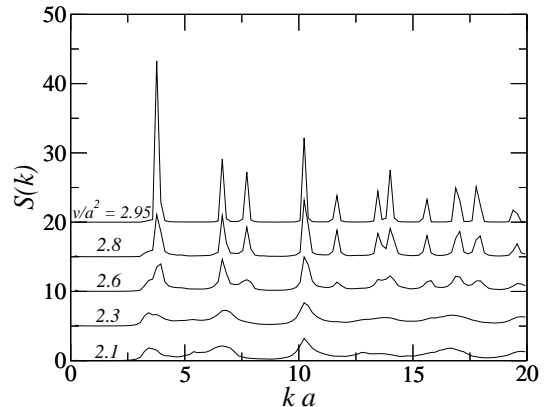


FIG. 9: Evolution of the averaged structure factor $S(k)$ with decreasing volume for the LDT-CH transformation with $w = 6$. Each curve corresponds to the configurations in Fig. 8 (a)-(e).

by quenching from the melt. This sample is then X-ray amorphous. Thus, we have here a sample that has WPIA.

The fact that this sample is X-ray amorphous, but still has within its structure some information of the parent crystalline phase from which it was obtained may be related to the so-called memory glass effect (MGE). The MGE was first identified in AlPO_4 berlinite,^{37,38} and then it was recognized to occur in a variety of materials such as SnI_4 and LiKSO_4 .² The effect consists in the amorphization of a sample under pressure, and the successive recovery of a crystalline sample, with the *same original orientation* upon decompression. In the following, some characteristics of the MGE for the present model system are studied.

The complete $v - P$ curves during volume controlled compression-decompression cycles are shown in Fig. 11 for different values of the final volume reached, v_{min} . The final configurations after the cycling are shown in Fig. 12. All the snapshots correspond to a recovered volume of $v/a^2 = 3.05$. Shown are the defects introduced by the cycling, corresponding to small regions of the different martensitic variants. Small dots correspond to the position of the particles. On a direct examination of the recovered structures, it is seen that the system has a tendency to recuperate its original orientation upon decompression. A closer inspection shows that the recovered LDT structure retains its initial orientation for high v_{min} , but becomes polycrystalline for lower v_{min} , losing the ‘memory’ of the initial orientation.

It is convenient to have a single parameter that measures the degree of memory of the structure. We take this parameter to be W , defined as

$$W = \frac{1}{36N} \sum_j \text{Re} \left[\sum_{k,k'} e^{\delta i(\alpha_{jk} - \alpha_{jk'})} \right], \quad (3)$$

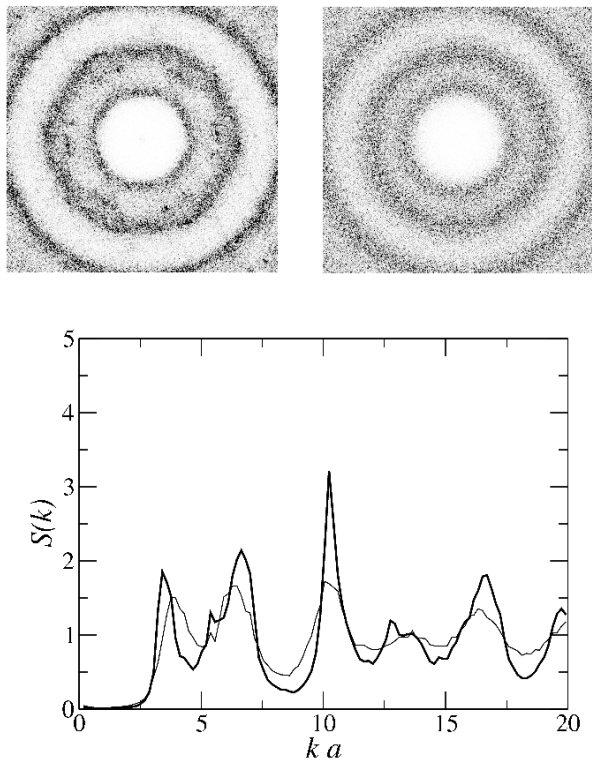


FIG. 10: Comparison of the structure factor corresponding to the sample obtained in the LDT-CH transformation [Fig. 8(e)] with a quenched amorphous structure at the same density. In the top the two-dimensional structure factors for the polycrystalline CH structure (left) and quenched amorphous structure (right) are shown. The angular averaged $S(k)$ is plotted at the bottom for the polycrystalline CH structure (bold continuous line) and quenched amorphous structure (thin continuous line).

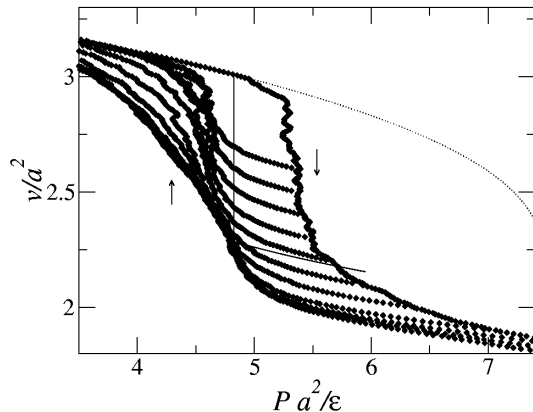


FIG. 11: $v - P$ compression-decompression cycles for different values of the final volume reached. From bottom to top v_{min}/a^2 goes from 1.6 to 2.6, in steps of 0.1. Dotted and thin continuous lines as in Fig. 7.

where k and k' are the nearest neighbors of particle j before and after the compression-decompression cycle, and $\alpha_{jk(k')}$ is the angle between $\vec{r}_{k(k')} - \vec{r}_j$ and an arbitrary reference direction. In particular, it can be seen that if the sample returns exactly to its initial configuration, we get $W = 1$. On the other hand, if the final local orientations in the sample are completely uncorrelated with the original ones, then $W = 0$. We take as the reference volume to compute W the value $v/a^2 = 3.05$ and the plot of W as a function of the minimum volume v_{min} reached during compression is seen in Fig. 13. We see in fact, that this number is close to one for $v_{min}/a^2 > 2$, whereas it is essentially zero when $v_{min}/a^2 < 1.9$. The memory of the system is lost continuously when v_{min} becomes lower, but note the interesting fact that for $v_{min} = 2.1$, in which there is no LDT phase left in the compressed sample (see Fig. 8), the value of W is still clearly different from zero. All the memory of the system here can be associated to the preferred orientation of the crystals of the CH phase, which in turn occurs because of the martensitic nature of the LDT-CH transition. As for this volume the sample is X-ray amorphous, this is an example of MGE.

VI. DISCUSSION AND CONCLUSIONS

We have studied a two dimensional model at $T = 0$ that displays a pressure driven martensitic transformation between a triangular structure (the austenite) with rotational C_6 symmetry, and a chain like structure (the martensite) with a lower (C_2) rotational symmetry. The martensite phase can be considered to be obtained from the austenite through a compression in one direction and an expansion in the perpendicular direction. The transformation occurs with an appreciable volume change. This is natural since pressure (which couples to volume in the free energy) is the driving force of the transformation.

The transition does not spontaneously occur at the equilibrium transformation pressure because an energy barrier exists. An excess pressure is needed to trigger the transformation. Defects in the original crystalline structure produce the appearance of ‘reaction paths’ which have (at the equilibrium pressure) relatively low energy barriers. These barriers vanish with a relatively low overpressure, triggering the transition. The necessary overpressure in the presence of defects is typically much smaller than that needed to destabilize the defect free structure. We have shown in particular, that vacancies are very effective in favoring the nucleation of three platelets related to the three variants of the martensite, which are however elastically distorted with respect to the ideal martensite. We call them pseudo-martensitic crystals.³⁰

After the nucleation of pseudo-martensite platelets, two different evolutions were observed. In one case, the pseudo-martensitic platelets find the way to become wedge shaped crystallites of the true martensitic structure. In this process, the internal stress of the martensite

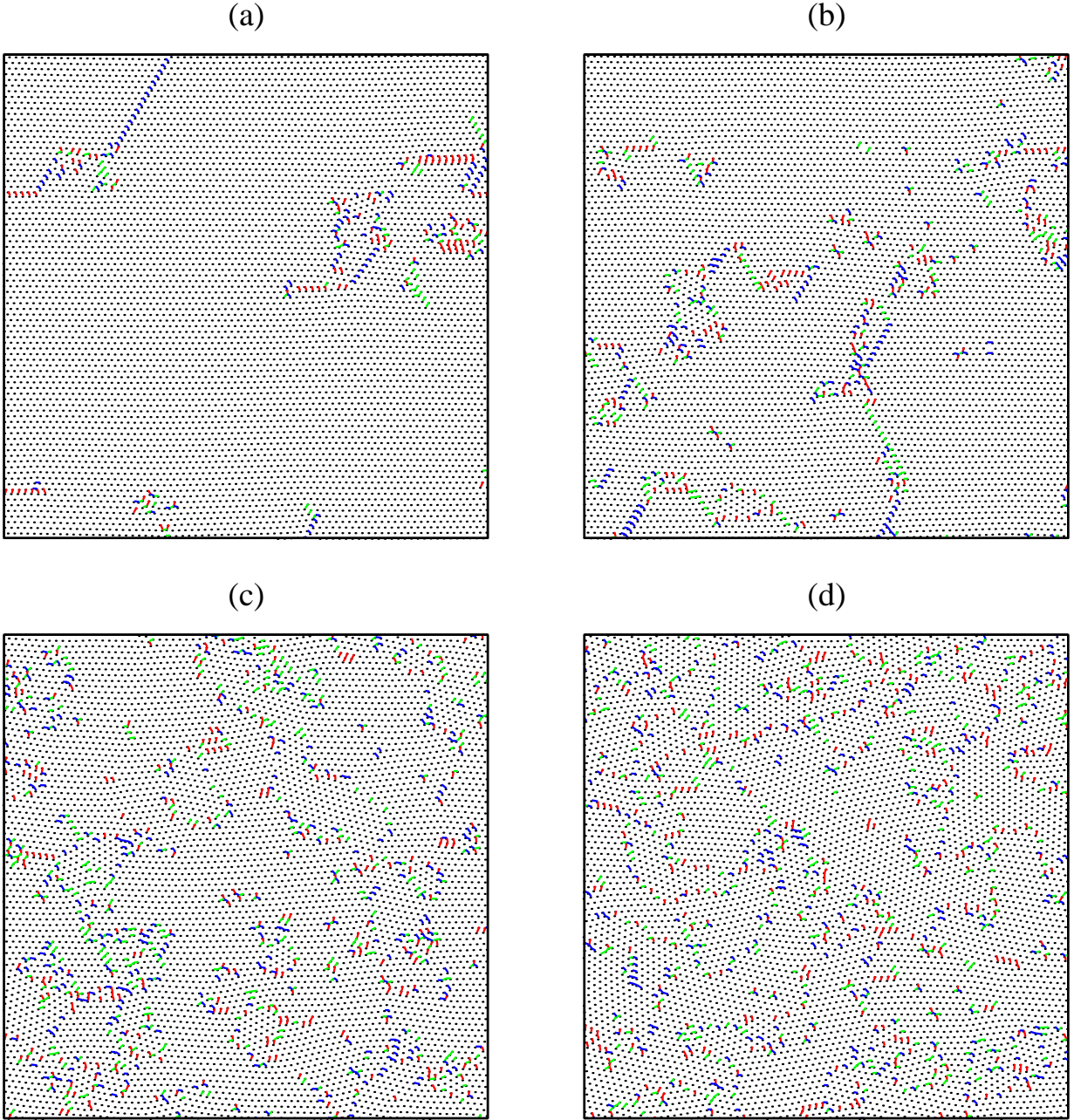


FIG. 12: (Color online) Snapshots of the system as recovered from the compression-decompression cycles shown in Fig. 11. All the snapshots correspond to a final volume of $v/a^2 = 3.05$. The minimum volumes reached are (a) $v/a^2 = 2.4$, (b) $v/a^2 = 2.2$, (c) $v/a^2 = 2.0$ and (d) $v/a^2 = 1.8$. Different colors indicate particles collapsed along each of the directions of the possible martensitic variants. Dots corresponding to the position of the particles are shown in order to identify the appearance of polycrystallinity.

relaxes, and the interface between austenite and martensite becomes very nearly the ideal invariant line of the transformation. These wedge shaped crystals grow upon volume decrease, until the whole sample consists of a collection of crystallites of the three different variants of the martensite, and no austenite remains. In this case, the

final size of the crystallites is expected to depend mainly on the density of defects in the system and the compression rate, since there are no other important limitations to martensite growth. In principle, very large crystal sizes can be obtained in samples with low concentration of defects driven at very a low compression rates.

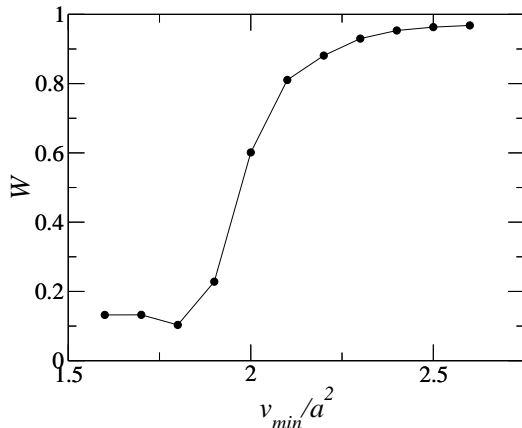


FIG. 13: The parameter W defined in Eq. (3) as a function of the minimum volume v_{min} reached in the compression-decompression cycles shown in Fig. 11.

In a second case, the conversion of pseudo-martensite to true martensite is strongly inhibited. In this case, upon compression, new platelets of pseudo-martensitic structure nucleate, that interact with preexisting ones. The structure obtained when the austenite has completely disappeared is much more disordered than in the previous case, and in particular, the final crystallite size in this case is expected to remain of the order of few interatomic distances. In some cases, the angularly averaged diffraction pattern of the final structure may well be taken by that of an amorphous structure. We have called this phenomenon weak pressure induced amorphization. This is not a true pressure induced amorphization since the final structure has a ‘memory’ of its parent crystal that is observable, for instance, in the full two-dimensional diffraction pattern. Upon decompression of this sample, a defective crystal is obtained, which, however, has a consistent tendency to be oriented in the same form as the original parent crystal. This is a description of the ‘memory glass effect’ (MGE), observed in different experimental situations.

The two different behaviors were obtained by changing the parameters of the interparticle potential. Concretely, the easy growth of the martensite was observed when the barrier between the two possible interparticle distances was small, whereas inhibited growth was observed when this barrier was higher.

Although the present model is not aiming to reproduce the characteristics of a specific real system with its complex interactions, some similarities concerning PIA, martensitic transformation and the MGE, may be addressed between this simple model system and real systems.

As we neglect temperature effects in our molecular dynamics simulation, the transformation between the austenite and martensite phases is of a mechanical nature

(and this should be qualitatively correct for any $T < T_g$). This means that the austenite is driven into a metastable region, until a mechanical instability limit is reached, and the martensite starts to nucleate spontaneously. Note the important fact (already present in our previous results in²⁶) that once nucleated, the interface between the two phases can propagate spontaneously, and this propagation, which occurs essentially at the sound velocity, is not limited by the diffusivity of the particles in any of the two bulk phases (which is zero here). In the case of defect free samples the mechanical instability of the austenite is signaled by the softening of a phonon mode. However, in the presence of defects the first mechanical instability corresponds to localized modes around the defects, and therefore it is not observable in the phonon spectrum. Thus, our present and previous²⁶ results reinforce our view that PIA is a mechanical transition, i.e. always triggered by mechanical instabilities. We find that defects can cause the transition pressure to be depressed to a value very close to the ideal thermodynamical equilibrium pressure between the two phases. We recognize however, that this result can be not universal but system dependent. The relevance of defects density in lowering the amorphization pressure was recently experimentally highlighted,³⁹ although whether the amorphization pressure approaches the extrapolated melting line upon introduction of more defects is not clear. The experimental evidence of amorphization occurring near the extrapolated melting line in some systems is at the base of a ‘thermodynamical’ scenario for PIA as directly related to the ‘thermodynamical melting’ mechanism at higher temperatures. We see that this evidence is also fully compatible with a mechanical mechanism.

A transformation reminiscent of our martensitic transformation with easy growth occurs between the high pressure phases of GaPO_4 . In this case, the low-cristobalite phase of GaPO_4 transforms to a $Cmcm$ structure on pressure loading.^{40,41} The transformation is of a displacive nature, and the mechanism consists of a fourfold-to-sixfold coordination change of the gallium coordination shell.⁴⁰ The peaks of the polycrystal are clearly identified, which indicates a large crystal size. In view of the results presented here, it could be interesting to exploit the martensitic point of view in analyzing this kind of pressure induced transformation.

On the other hand, the transformation in the case of blocked growth is in line with investigations of the high pressure transformations of AlPO_4 and the MGE.^{42,43,44,45,46} What was first viewed as a true PIA with MGE, was later identified as a crystal-crystal pressure-induced transformation between a berlinite AlPO_4 structure and a $Cmcm$ polycrystalline structure with very small crystal size, i.e., in our language, a WPIA. Carefully done molecular dynamics simulations⁴³ and X-ray experiments⁴⁴ have identified some peaks of the X-ray diffraction patterns of the high pressure phase as corresponding to the $Cmcm$ structure. In addition, recent work has been devoted to establish that the $Cmcm$

structure is the stable one at high pressures,⁴⁶ but little is known about the mechanism of the transformation. In view of the similarities between the MGE in our two-dimensional model and in the AlPO_4 case, we suggest that MGE occurs simply as a consequence of the amorphization being only of the weak type, instead of a true one. Furthermore, we speculate that the mechanism of the berlinite- $Cmcm$ transformation in AlPO_4 could be very similar to the mechanism of the low cristobalite- $Cmcm$ transformation in GaPO_4 . However, the growth of the $Cmcm$ structure over the berlinite phase of AlPO_4 could be inhibited by energetic barriers, leading to the polycrystal with very small crystal size.

To conclude, we notice how the present model, although highly simplified and not representing any particular real system, captures much of the phenomenology observed in a variety of real cases. As such, it is an important theoretical tool to guide the analysis of concrete cases. We expect to be able to go further in this direction in the future.

Acknowledgments

S.B. is financially supported by CONICET (Argentina), and also acknowledges the hospitality of The Abdus Salam ICTP (Trieste), where part of this work was done.

APPENDIX: STRESS DEPENDENT ELASTIC CONSTANTS AND THEIR STATIC LIMIT

Fluctuation formulas for stress-free elastic constants in the NVT ensemble are given by³³

$$C_{ijkl} = \frac{2NkT}{V} (\delta_{ij}\delta_{jk} + \delta_{ik}\delta_{jl}) - \langle (P_{ij}P_{kl}) - \langle P_{ij} \rangle \langle P_{kl} \rangle \rangle + B_{ijkl}, \quad (\text{A.1})$$

where N is the number of particles, k is the Boltzmann constant, T is the temperature and V is the volume of the system. The brackets, $\langle \dots \rangle$, denotes ensemble averages. P_{ij} are the components of the pressure tensor given by

$$P_{ij} = \frac{1}{V} \left(\sum_{\alpha} \frac{p_{(i)\alpha} p_{(j)\alpha}}{m_{\alpha}} - \sum_{\alpha < \beta} \frac{V'(r_{\alpha\beta})}{r_{\alpha\beta}} r_{(i)\alpha\beta} r_{(j)\alpha\beta} \right), \quad (\text{A.2})$$

with α and β particle running indexes, $p_{(i)\alpha}$ the momentum of the particle α (with mass m_{α}) in the i direction, and $r_{\alpha\beta}$ the distance between particles, with component $r_{(i)\alpha\beta}$ in the i direction. Finally,

$$B_{ijkl} = \frac{1}{V} \left\langle \sum_{\alpha < \beta} \left(\frac{V''(r_{\alpha\beta})}{r_{\alpha\beta}^2} - \frac{V'(r_{\alpha\beta})}{r_{\alpha\beta}^3} \right) \times \right.$$

$$\left. \times r_{(i)\alpha\beta} r_{(j)\alpha\beta} r_{(k)\alpha\beta} r_{(l)\alpha\beta} \right\rangle. \quad (\text{A.3})$$

Here, $V'(r)$ and $V''(r)$ correspond to first and second derivatives of the interaction potential energy at r .

Consider the static (zero temperature) limit. In this limit one has to consider only the perfect crystal structure without any thermal fluctuation. In this case the first term of Eq. (A.1), proportional to the temperature, vanishes. The second term, which measures the fluctuation of the pressure tensor, vanishes too. Besides, the term containing the momentum of the particles in Eq. (A.2) is zero, and $C_{ijkl} = B_{ijkl}$. Then, in this limit, the calculation of the elastic constant is straightforward, and instead of using the complete fluctuation formulas, which needs an ensemble average to be performed, we use the static limit Eq. (A.3) calculated over a given sample.

Let us consider, for instance, the calculation of C_{12} in a triangular structure of lattice parameter r with nearest neighbors interactions only.

$$\begin{aligned} C_{12} &= \frac{1}{2V} \sum_{\alpha, \beta=1}^N \left(V''(r_{\alpha\beta}) - \frac{V'(r_{\alpha\beta})}{r_{\alpha\beta}} \right) \frac{r_{(x)\alpha\beta}^2 r_{(y)\alpha\beta}^2}{r_{\alpha\beta}^2} \\ &= \frac{1}{2V} \left(V''(r) - \frac{V'(r)}{r} \right) \frac{1}{r^2} \sum_{\alpha=1}^N 4 \left(\frac{r}{2} \right)^2 \left(\frac{\sqrt{3}}{2} r \right)^2 \\ &= \frac{1}{2V} \left(V''(r) - \frac{V'(r)}{r} \right) N \frac{3}{4} r^4 \\ &= \frac{\sqrt{3}}{4} \left(V''(r) - \frac{V'(r)}{r} \right), \end{aligned} \quad (\text{A.4})$$

where we used $N/V = 2/(\sqrt{3}r^2)$. Analogously we obtained

$$C_{11} = \frac{3}{4} \sqrt{3} \left(V''(r) - \frac{V'(r)}{r} \right), \quad (\text{A.5})$$

and

$$P = -\sqrt{3} \frac{V'(r)}{r}. \quad (\text{A.6})$$

The stress dependent shear modulus is given by

$$G' = \frac{C_{11} - C_{12}}{2} - P = \frac{\sqrt{3}}{4} \left(V''(r) + 3 \frac{V'(r)}{r} \right). \quad (\text{A.7})$$

Then, the condition of vanishing stress dependent shear modulus coincides with condition (2) in the static limit.

-
- ¹ E. G. Ponyatovsky and O. I. Barkalov, *Mater. Sci. Rep.* **8**, 147 (1992).
- ² S. M. Sharma and S. K. Sikka, *Prog. Mater. Sci.* **40**, 1 (1996).
- ³ P. Richet and P. Gillet, *Eur. J. Mineral.* **9**, 907 (1997).
- ⁴ K. J. Kingma, R. J. Hemley, H. Mao, and D. R. Veblen, *Phys. Rev. Lett.* **70**, 3927 (1993).
- ⁵ E. Gregoryanz, R. J. Hemley, H. K. Mao, and P. Gillet, *Phys. Rev. Lett.* **84**, 3117 (2000).
- ⁶ J. Haines, J. M. Léger, F. Gorelli, and M. Hanfland, *Phys. Rev. Lett.* **87**, 155503 (2001).
- ⁷ Z. Nishiyama, *Martensitic Transformations* (Academic Press, New York, 1978).
- ⁸ O. Mishima, *Nature (London)* **384**, 546 (1996).
- ⁹ A. G. Lyapin and V. V. Brazhkin, *Phys. Rev. B* **54**, 12036 (1996).
- ¹⁰ J. Badro, P. Gillet, and J.-L. Barrat, *Europhys. Lett.* **42**, 643 (1998).
- ¹¹ J. S. Tse, D. D. Klug, C. A. Tulk, I. Swainson, E. C. Svensson, C.-K. Loong, V. Shpakov, V. R. Belosludov, R. V. Belosludov, and Y. Kawazoe, *Nature (London)* **400**, 647 (1999).
- ¹² E. L. Gromnitskaya, O. V. Stal'gorova, V. V. Brazhkin, and A. G. Lyapin, *Phys. Rev. B* **64**, 094205 (2001).
- ¹³ D. Wolf, P. R. Okamoto, S. Yip, J. F. Lutsko, and M. Kluge, *J. Mater. Res.* **5**, 286 (1990).
- ¹⁴ J. R. Chelikowsky, H. E. King Jr, N. Troullier, J. L. Martins, and J. Glinnemann, *Phys. Rev. Lett.* **65**, 3309 (1990).
- ¹⁵ A. D. Pomponio and A. Continenza, *Phys. Rev. B* **50**, 5950 (1994).
- ¹⁶ S. Tsuneyuki, Y. Matsui, H. Aoki, and M. Tsukada, *Nature (London)* **339**, 209 (1989).
- ¹⁷ B. W. H. van Beest, G. J. Kramer, and R. A. van Santen, *Phys. Rev. Lett.* **64**, 1955 (1990).
- ¹⁸ N. Binggeli, J. R. Chelikowsky, and R. M. Wentzcovitch, *Phys. Rev. B* **49**, 9336 (1994).
- ¹⁹ P. C. Hemmer and G. Stell, *Phys. Rev. Lett.* **24**, 1284 (1970).
- ²⁰ G. Stell and P. C. Hemmer, *J. Chem. Phys.* **56**, 4274 (1972).
- ²¹ E. A. Jagla, *Phys. Rev. E* **58**, 1478 (1998).
- ²² M. R. Sadr-Lahijany, A. Scala, S. V. Buldyrev, and H. E. Stanley, *Phys. Rev. Lett.* **81**, 4895 (1998).
- ²³ E. A. Jagla, *J. Chem. Phys.* **111**, 8980 (1999).
- ²⁴ E. A. Jagla, *Phys. Rev. E* **63**, 061509 (2001).
- ²⁵ A. Scala, M. R. Sadr-Lahijany, N. Giovambattista, S. V. Buldyrev, and H. E. Stanley, *Phys. Rev. E* **63**, 041202 (2001).
- ²⁶ S. Bustingorry and E. A. Jagla, *Phys. Rev. B* **69**, 064110 (2004).
- ²⁷ M. P. Allen and D. J. Tildesley, *Computer Simulation of Liquids* (Clarendon Press, Oxford, 1987).
- ²⁸ J. M. Haile, *Molecular Dynamics Simulation: Elementary Methods* (Wiley, New York, 1992).
- ²⁹ E. A. Jagla, *J. Chem. Phys.* **110**, 451 (1999).
- ³⁰ R. C. Pond, S. Celotto, and J. P. Hirth, *Acta. Mater.* **51**, 5385 (2003).
- ³¹ M. Born and K. Huang, *Dynamical Theory of Crystal Lattices* (Clarendon, Oxford, 1956).
- ³² H. Wang, S. Yip, S. R. Phillpot, and D. Wolf, *Phys. Rev. Lett.* **71**, 4182 (1993).
- ³³ Z. Zhou and B. Joós, *Phys. Rev. B* **54**, 3841 (1996).
- ³⁴ Next nearest neighbors interactions may eventually produce the instability to appear at some finite wave vector. If this is the case, then the instability will not be seen in the elastic constants, which are the long wavevector limit of the phonon spectrum.
- ³⁵ Note that this situation is much more restrictive than what is usually called in the literature a 'reversible amorphization' transition. A reversible amorphization is usually meant to occur when a system passes from crystalline to amorphous upon compression, and becomes crystalline again upon decompression, without requiring any kind of 'memory' between the initial and final crystal states. In this sense, all the results presented here show 'reversible' amorphization. It has to be mentioned that we can obtain with our model 'irreversible' amorphization (in which the sample remains amorphous when pressures is released) by the inclusion in the interaction potential of an attractive term among the particles, as discussed in Ref. [22]. To avoid confusion, we do not use the term 'reversible' in the text.
- ³⁶ T. Yamanaka, T. Nagai, and T. Tsuchiya, *Z. Kristallogr.* **212**, 401 (1997).
- ³⁷ M. B. Krueger and R. Jeanloz, *Science* **249**, 647 (1990).
- ³⁸ J. S. Tse and D. D. Klug, *Science* **255**, 1559 (1992).
- ³⁹ G. P. Johari and O. Andersson, *Phys. Rev. B* **70**, 184108 (2004).
- ⁴⁰ J. L. Robeson, R. R. Winters, and W. S. Hammack, *Phys. Rev. Lett.* **73**, 1644 (1994).
- ⁴¹ S. M. Sharma and S. K. Sikka, *Phys. Rev. Lett.* **74**, 3301 (1995).
- ⁴² K. J. Kingma, R. J. Hemley, H. Mao, and D. R. Veblen, *Phys. Rev. Lett.* **72**, 1302 (1994).
- ⁴³ N. Garg and S. M. Sharma, *J. Phys.: Condens. Matter* **12**, 372 (2000).
- ⁴⁴ S. M. Sharma, N. Garg, and S. K. Sikka, *Phys. Rev. B* **62**, 8824 (2000).
- ⁴⁵ P. Gillet, J. Badro, B. Varrel, and P. F. McMillan, *Phys. Rev. B* **51**, 11262 (1995).
- ⁴⁶ L. M. Ramaniah, S. M. Sharma, K. Kunc, N. Garg, and M. Laghate, *Phys. Rev. B* **68**, 014119 (2003).